

AD-A084 810

AIR FORCE GEOPHYSICS LAB HANSCOM AFB MA
LARGE SPACE STRUCTURE CHARGING DURING ECLIPSE PASSAGE.(U)
JAN 80 D H GAUNT
AFGL-TR-80-0022

F/G 22/2

UNCLASSIFIED

NL

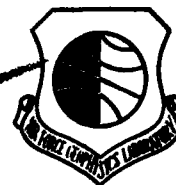
1 OF 1
AD
A084 810

END
DATE
FILMED
6-80
DTIC

AFGL-TR-80-0022
AIR FORCE SURVEYS IN GEOPHYSICS, NO. 420

LEVEL *14*

12



ADA084810

**Large Space Structure
Charging During Eclipse Passage**

DAVID M. GAUNTT

15 January 1980

DTIC
ELECTE
MAY 28 1980
S D C

Approved for public release; distribution unlimited.

DDC FILE COPY

SPACE PHYSICS DIVISION PROJECT 7661
AIR FORCE GEOPHYSICS LABORATORY
HANSCOM AFB, MASSACHUSETTS 01731

AIR FORCE SYSTEMS COMMAND, USAF

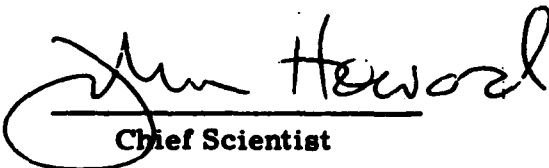


80 28 003

This report has been reviewed by the ESD Information Office (OI) and is releasable to the National Technical Information Service (NTIS).

This technical report has been reviewed and is approved for publication.

FOR THE COMMANDER


Chief Scientist

Qualified requestors may obtain additional copies from the Defense Documentation Center. All others should apply to the National Technical Information Service.

Unclassified

SECURITY CLASSIFICATION OF THIS PAGE (When Data Entered)

REPORT DOCUMENTATION PAGE		READ INSTRUCTIONS BEFORE COMPLETING FORM
1. REPORT NUMBER AFGL-TR-80-0022	2. GOVT ACCESSION NO. AD A084 810	3. SPECIFIC CATALOG NUMBER
4. TITLE (and Subtitle) LARGE SPACE STRUCTURE CHARGING DURING ECLIPSE PASSAGE		5. TYPE OF REPORT & PERIOD COVERED Scientific. Interim.
7. AUTHOR(s) David M. Gauntt		6. PERFORMING ORG. REPORT NUMBER AFSG No. 420
9. PERFORMING ORGANIZATION NAME AND ADDRESS Air Force Geophysics Laboratory (PH) Hanscom AFB Massachusetts 01731		8. CONTRACT OR GRANT NUMBER(s)
11. CONTROLLING OFFICE NAME AND ADDRESS Air Force Geophysics Laboratory (PH) Hanscom AFB Massachusetts 01731		10. PROGRAM ELEMENT, PROJECT, TASK AREA & WORK UNIT NUMBERS 62101F 76610803
14. MONITORING AGENCY NAME & ADDRESS (if different from Controlling Office)		12. REPORT DATE 15 January 1980
		13. NUMBER OF PAGES 39
		15. SECURITY CLASS (of this report) Unclassified
		15a. DECLASSIFICATION DOWNGRADING SCHEDULE
16. DISTRIBUTION STATEMENT (of this Report) Approved for public release; distribution unlimited.		
17. DISTRIBUTION STATEMENT (of the abstract entered in Block 20, if different from Report)		
18. SUPPLEMENTARY NOTES		
19. KEY WORDS (Continue on reverse side if necessary and identify by block number) Spacecraft charging Large space structures Geosynchronous orbit		
20. ABSTRACT (Continue on reverse side if necessary and identify by block number) Much work has been devoted to the study of the differential charging of geosynchronous spacecraft, primarily that charging caused by injection events and uneven illumination of isolated surfaces. However, as the lack of illumination in the penumbra eliminates the latter problem, little attention has been paid to charging during eclipse passage. For a sufficiently large structure (length greater than 1 km), the gradient of illumination in the penumbra is large enough to contribute significantly to differential charging.		

DD FORM 1 JAN 73 1473

EDITION OF 1 NOV 65 IS OBSOLETE

Unclassified

SECURITY CLASSIFICATION OF THIS PAGE (When Data Entered)

Unclassified

SECURITY CLASSIFICATION OF THIS PAGE (When Data Entered)

20. Abstract (Continued)

In this paper, three main subjects will be discussed: (1) the causes of charging at geosynchronous altitudes; (2) a simple model of the plasma from which the differential charging equations can be derived; and (3) the results of a computer program based on these equations, together with several theoretically fit sets of equations to approximate the results.

SECURITY CLASSIFICATION OF THIS PAGE (When Data Entered)

Accession For	
MTLS	SPALI
EDC TAB	
Unannounced	
Justification	
By	
Distribution/	
Availability Codes	
Dist.	Avail and/or special
A	.

Contents

1. INTRODUCTION	5
2. BASIC THEORY	6
3. RESULTS	8
4. THEORETICAL FIT	17
5. CONCLUSION	21
REFERENCES	23
APPENDIX A: Current Values as Functions of Voltage, Number Density, and Temperature	25

Illustrations

1. Observed ATS-5 Potentials in Eclipse vs Potentials Predicted by Program SHADOW	8
2a. Potential During Eclipse Passage V_o Normalized by the Potential in Eclipse V_{max} as a Function of the Minimum Ray Path Height X_m to the Center of the Sun	9
2b. Potential During Eclipse Passage for Predicted V_o/V_{max} Values Using SHADOW	10
3a. Parameter X_m Measurement	11
3b. Solar Power Satellite Schematic Showing Coordinate System and Electrical Analog for Simulation Purposes	11

Illustrations

4. Plot of Eclipse Potentials Determined for 21 ATS-5 Events Employing a Planar (thin sheath) or Point (thick sheath) Approximation	12
5. Potential Drop Across a 10-km Solar Power Satellite with Its Center at $X_0 = 150$ km	13
6. Potential Drops Normalized by Dividing by the Total Potential Drop Across the Solar Power Satellite to Show Variation in Potential Across the Structure More Clearly	13
7. Maximum Potential Drop Across a Solar Power Satellite Located at 150 km	14
8. Maximum Voltage Drop Across the Solar Power Satellite (and Space Based Radar) for Various Plasma Conditions and Sheath Assumptions	15
9. Maximum Voltage Drops at $X_0 = -150$ km for the 21 ATS-5 Plasma Events as a Function of V_{max} , the Eclipse Potential	15
10. Ohmic Power Loss in Solar Power Satellite as a Function of Resistivity	16

Tables

1. Space Plasma Parameters from ATS-5	13
---------------------------------------	----

Large Space Structure Charging During Eclipse Passage

1. INTRODUCTION

The large variations in spacecraft potential measured relative to the plasma that have been observed¹ are believed to be the result of the dominance of the electron flux. This may be explained as follows. According to Garrett,² the two plasma populations, protons and electrons, can each be characterized as a pair of Maxwellian populations:

$$f(V) = N \left(\frac{m}{2\pi kT} \right)^{3/2} \exp \left(\frac{-mv^2}{2kT} \right) \quad (1)$$

each of which has a number density (N) and a Maxwellian temperature (T). The energy of each particle is proportional to the mass of the particle and the square of its velocity; thus, for a given energy, protons, being three orders of magnitude more massive than electrons, have velocities 43 times lower. Temperature and number flux, being comparable on the macroscopic scale to energy and velocity on

(Received for publication 15 January 1980)

1. DeForest, S. E. (1972) Spacecraft charging at synchronous orbit, J. Geophys. Res. 77(No. 4):651.
2. Garrett, H. B. (1977) Modeling of the Geosynchronous Plasma Environment, AFGL-TR-77-0288, AD A053 164.

the microscopic, have a similar relationship, leading to the dominance of the electron flux.

Under the influence of only these hot Maxwellian plasmas (kT greater than 10^2 eV), any object in the plasma absorbing charged particles would collect a net negative charge, attaining an electric potential large enough to repel the incident electron flux (-10 V to $-20,000$ V). However, other effects can change the situation. If an additional dense "cold" plasma population (kT less than 10 eV, N greater than 10 n/cm³) is present, then any negative voltage is neutralized by an enhanced ion flux. This effect suppresses charging in low earth orbit³ but not at geosynchronous altitudes, where the cold population is extremely thin ($N = 10^{-2}$ n/cm³). When the structure is illuminated (for example, a satellite in the sunlight), electrons are removed from the surface by the photoelectric effect. Often this photoelectron current dominates the ambient electron current, resulting in a small positive potential (0.1 to 10.0 V).⁴

As a small satellite passes from eclipse, its voltage will undergo a drastic change (~ 1000 V in 1 min), corresponding to the change in illumination.⁵ If it is large, as mentioned earlier, the gradient of illumination will lead to a voltage differential across the surface. As will be seen, the magnitude of this differential potential will range from 10^{-3} to 10^3 V for a 10-km structure.

2. BASIC THEORY

If J_p is the total current density to a small spacecraft, then¹

$$J_p = J_e - (J_i + J_{se} + J_{si} + J_{bs}) + J_{th} - J_{pe} \frac{A_c}{A_s} \quad (2)$$

where

J_e = the ambient electron current density

J_i = the ambient ion current density

J_{se} = the secondary electron current density caused by primary ambient electrons

J_{si} = the secondary electron current density caused by primary ambient ions

3. Whipple, E. C. (1965) The Equilibrium Electric Potential of a Body in the Upper Atmosphere, NASA X-615-65-296.
4. Garrett, H. B., Pavel, A. L., and Hardy, D. A. (1977) Rapid Variations in Spacecraft Potential, AFGL-TR-77-0132, AD A046 350.
5. Rosen, A. (1975) Spacecraft Charging: Environment Induced Anomalies, Paper 75-91, AIAA 13th Aerospace Sciences Meeting.

J_{bs} = the backscatter electron current density

J_{th} = the "thruster" current density, caused by ion drive, plasma beams, etc.

J_{pe} = the photoelectron current density

A_c = the sunlit cross-section area of the spacecraft, and

A_s = the surface area of the spacecraft

The corresponding values for J_e , J_i , J_{se} , J_{si} , J_{pe} , and J_{bs} as functions of voltage, number density, and temperature have been derived by Tsipouras and Garrett⁶ (assuming a thick plasma sheath, an isotropic, two-Maxwellian plasma, and an aluminum surface); these values are listed in the Appendix. The thruster current density has been assumed to be zero for this study, and any capacitance, inductance, or local differential charging effects are ignored. For a system in equilibrium, the plasma current I_p^* (that is, the plasma current density J_p multiplied by the surface area A_s) will be equal to zero, defining by Eq. (2) a unique voltage for a given situation that will be the potential on the spacecraft as measured relative to the plasma. While the currents are time varying, the time constant for Eq. (2) to be satisfied is on the order of milliseconds,⁷ and the assumption of equilibrium is justified.

The extension to a large structure such as a space based radar (SBR) or solar power satellite (SPS) is made by two changes in Eq. (2). First, the ambient plasma equations change, attenuating the number flux of the attracted species (thin sheath approximation); that is, the current of the attracted species is assumed to be independent of the voltage; there is no change in the repelled species (see Appendix). Second, an ohmic current, the current gained or lost to other parts of the spacecraft, is added to Eq. (2). Equation (3) now gives the net current to a particular surface, or node of the spacecraft:

$$I_n = I_{p*} + I_{ohm} \quad (3)$$

* (Please note that any future reference to I_p includes the ambient plasma, secondary electron, backscattered electron, and photoelectron currents; similar conventions hold for J_p , and the phrases "plasma current" and "plasma current density." Also, direction of current flow is taken to be the direction of electron flow, and potentials are measured relative to the plasma.)

6. Tsipouras, P., and Garrett, H. B. (1979) Spacecraft Charging Model - Two Maxwellian Approximation, AFGL-TR-79-0153, AD A077 907.

7. Rothwell, P. L., Rubin, A. G., and Yates, G. K. (1977) A simulation model of time-dependent plasma spacecraft interactions, Proc. of the Spacecraft Charging Conference, AFGL-TR-77-0051/NASA TMX-73537.

where

I_n = the total current to the node

I_{ohm} = the ohmic current to the node

I_p = the plasma current to the node [Eq. (2)]

Since the structure is assumed to be in equilibrium as before, the current to each node must be equal to zero. Finding the set of voltages for which this is true constitutes the solution to the charging problem.

3. RESULTS

A set of equations defined by Eqs. (2) and (3) was solved by program SHADOW using iterative means on the CDC 6600 system at AFGL, Hanscom AFB. Figure 1 presents the results for Eq. (2) (that is, a single node). The horizontal axis represents actual potentials observed by the NASA geosynchronous satellite ATS-5 during 21 eclipses from 1969 to 1970; the vertical axis represents the potentials predicted by SHADOW. The points plotted fall close to the identity line, and have a standard deviation of about 1200 volts, confirming the validity of SHADOW in calculating satellite potentials.

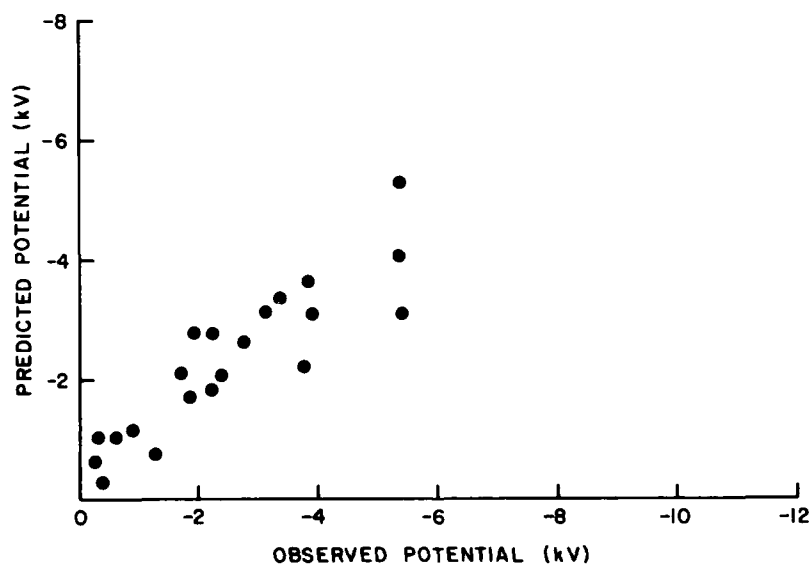


Figure 1. Observed ATS-5 Potentials in Eclipse versus Potentials Predicted by Program SHADOW

Figure 2 is a plot of the single point satellite potentials V_o normalized to the shadow potential V_{max} against position in orbit X_m .⁸ This parameter X_m is defined as the minimum altitude of the central ray of the disk of the sun as seen from the satellite (Figure 3a). The model used to describe the illumination of the spacecraft as a function of X_m , $F(X_m)$, assumes no attenuation due to the atmosphere, an earth radius of 6378 km, and an apparent solar radius of 185.2 km (see Appendix for formula). Figure 2a is a plot of the observed potentials (normalized by the eclipse potentials V_o) as the satellite ATS-5 entered or left eclipse, whereas Figure 2b is a plot of the potentials predicted by the program SHADOW, assuming a photoelectric current density of 0.4 nA/cm^2 (or $4 \cdot 10^{-6} \text{ A/m}^2$), the plasma conditions observed by ATS-5, a roughly spherical probe. The shape of the satellite is important in determining the ratio A_c/A_s of Eq. (2).

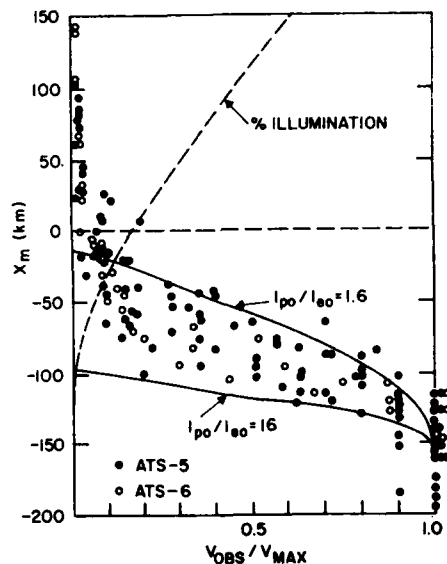


Figure 2a. Potential During Eclipse Passage, V_o , Normalized by the Potential in Eclipse, V_{max} , as a Function of the Minimum Ray Path Height, X_m , to the Center of the Sun. Twenty-one examples of actual ATS-5 and ATS-6 plasma observations during eclipse passage are plotted

8. Garrett, H. B., and Rubin, A. G. (1978) Spacecraft charging at geosynchronous orbit-generalized solution for eclipse passage, Geophys. Res. Lettrs. 5(No. 10):865.

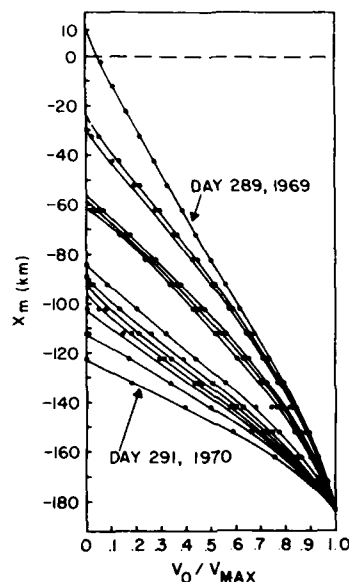


Figure 2b. Potential During Eclipse Passage for Predicted V_0/V_{max} Values Using SHADOW

Next a series of runs was done for several SPS (Solar Power Satellite) and SBR (Space Based Radar) models. Each structure was broken into a series of segments or nodes, and the potential on each node found. The structures were assumed to be 10 km across, with a thickness of 1 cm. Each structure was divided into a series of 10 to 100 nodes, each with the same width and approximately uniform illumination (Figure 3b). The structures were also assumed to be homogeneous with the surface properties (photoelectron, secondary emission, etc.) of ATS-5. The conductivity, number of nodes, and plasma parameters were varied in order to test the numerical sensitivity of the program (10 nodes gave results accurate to ~ 2 percent of the 100-node model). A wide variety of information was extracted from each run. To list a few: the potential, ohmic energy dissipation, the ohmic current at each point in the structure, and the total voltage drop and energy dissipation across the structure.

The potentials in the penumbra, based on a thin sheath approximation, tend to be twice the magnitude of those potentials predicted using the thick sheath approximation (Figure 4). This is a direct result of the attenuation of the attracted species in the thin sheath approximation. Also, the potential gradients were

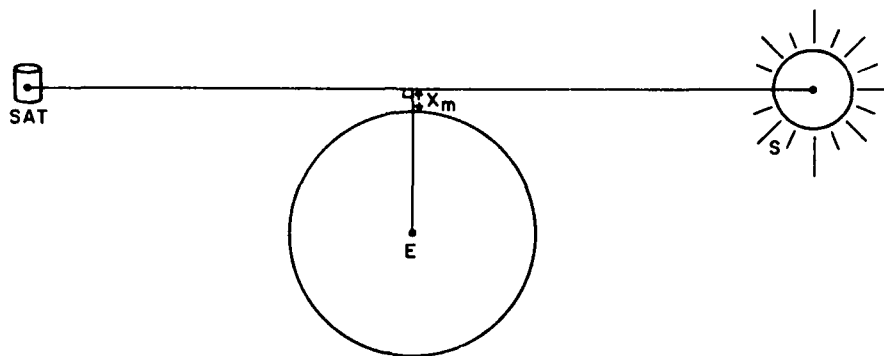


Figure 3a. Illustration of Parameter X_m Measurement. Note that X_m is the height of the minimum ray path to the center of sun (S) above the center of earth (E) as seen by the satellite (SAT)

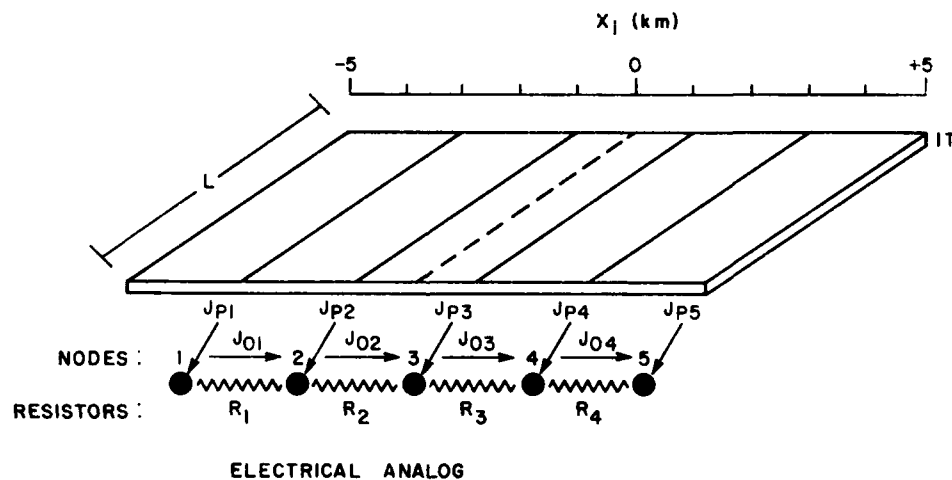


Figure 3b. Solar Power Satellite Schematic Showing Coordinate System and Electrical Analog for Simulation Purposes

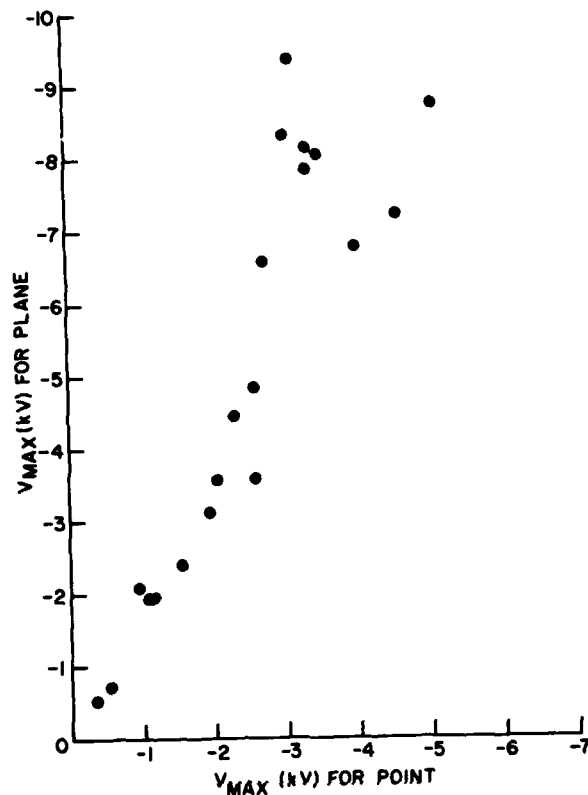


Figure 4. Plot of Eclipse Potentials Determined for 21 ATS-5 Events Employing a Planar (thin sheath) or Point (thick sheath) Approximation

greatly affected by the ohmic currents for low resistance models, differing by as much as 500 V from the high resistance potentials. The potentials for a poorly conducting surface are more positive toward the high X_m end (sunlit) than for a good conductor, whereas those toward the low X_m end (shadowed) tend to be more negative. This, of course, is due to the characteristic uniform potential of a perfect conductor. This latter potential, measured relative to the plasma, can be easily determined by using the average value of the photoelectron current density $J_{peo} \cdot F(X_m)$ across the structure in a single point, thin sheath potential calculation.

The results of calculations using ATS-5 data from Day 289, 1969 (a particularly severe day for charging) at $X_0 = -150$ km are plotted in Figures 5 to 10. Figure 5 shows the potential drop relative to the shadowed end of the SPS for five different resistances (see Table 1 for plasma parameters). In Figure 6 these potentials have been normalized by dividing by the total drop between the ends of the structure ΔV . The high-resistance curve is nearly linear, owing to the fact

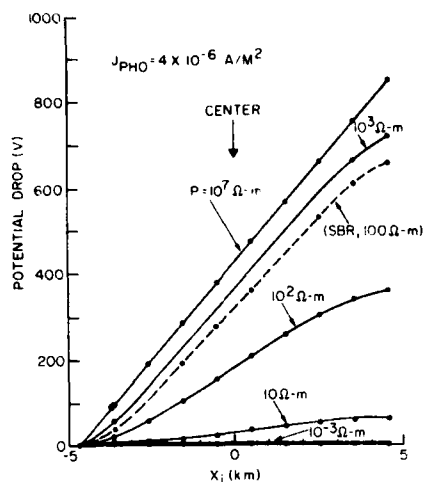


Figure 5. Potential Drop Across a 10-km Solar Power Satellite with its Center at $X_0 = 150$ km. Various values of the conductance have been assumed while the ambient conditions were those measured by ATS-5 on Day 289, 1969. The dashed line is a similar plot for the Space Based Radar

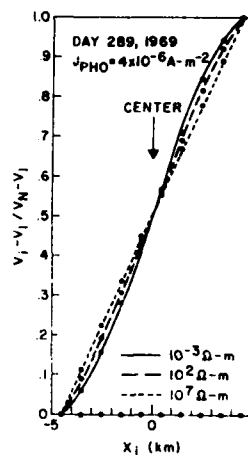


Figure 6. The Potential Drops in Figure 5 are Redrawn, Normalized by Division by the Total Potential Drop across the Solar Power Satellite to Show Variation in Potential Across the Structure More Clearly

Table 1. Space Plasma Parameters From ATS-5

Entity	Day 289, 1969		Day 291, 1970	
	N (cm ⁻³)	T (eV)	N (cm ⁻³)	T (eV)
Electrons	0.292	1060	0.835	998
	0.550	6070	0.227	3910
Ions	0.057	103	0.276	319
	0.690	8090	0.911	9530

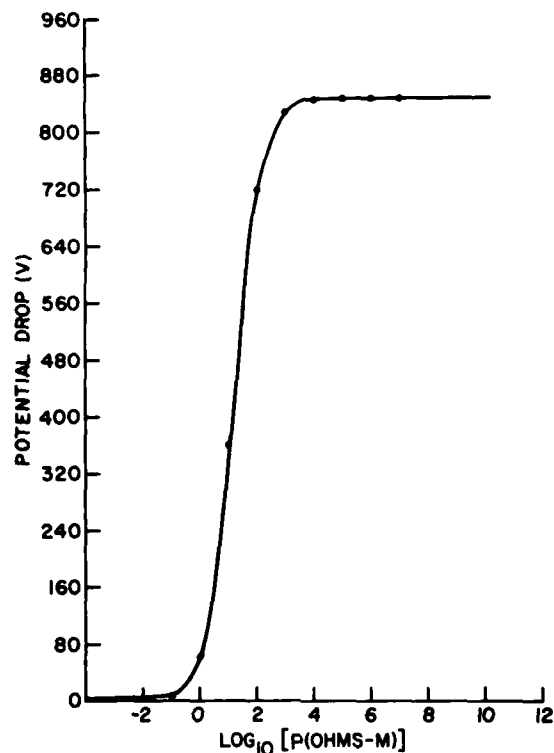


Figure 7. Maximum Potential Drop Across a Solar Power Satellite Located at 150 km

that $F(X_m)$ is linear to the first order over the length of the structure at ~ 150 km. The low-resistance curves show a definite S-shape. Also plotted in Figure 5 are potentials for a circular 10-km diam structure (SBR model) compared to the square SPS. This curve has been compared for a resistivity of $10^3 \Omega\text{-m}$ for the same conditions as the SPS. There is little difference in this and the corresponding SPS curve; however, the potential drop of the SBR is less, most likely a result of the reduced SBR area compared to the SPS.

The effect of resistance on the total voltage drop is plotted in Figure 7. The vertical axis is the voltage drop; the horizontal axis is the common logarithm of resistance in ohms for a 10-km structure at $X_m = -150$ km, again for Day 289 of 1969. The change from a conductor to nonconductor occurs for resistivities of 10^0 to $10^5 \Omega\text{-m}$, roughly the resistivity of semiconductors.

Figure 8 is a plot of the voltage drop against X_m for a resistance of $10^7 \Omega\text{-m}$ for the plasma conditions on Day 289, 1969 and Day 291, 1970, and assumes a point or plane. Figure 9 is the potential drop against the maximum potential V_{\max} in

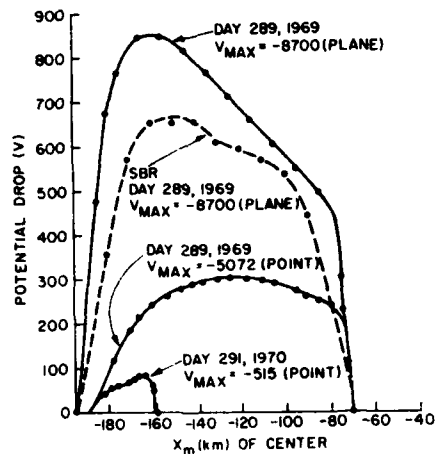


Figure 8. Maximum Voltage Drop Across the Solar Power Satellite (and Space Based Radar) for Various Plasma Conditions and Sheath Assumptions

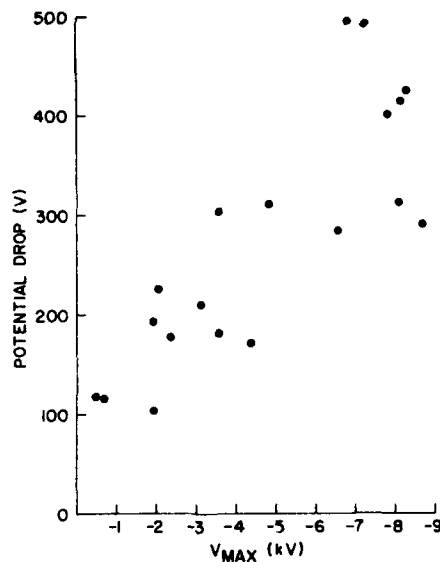


Figure 9. Maximum Voltage Drops at $X_0 = -150$ km for the 21 ATS-5 Plasma Events as a Function of V_{max} , the Eclipse Potential

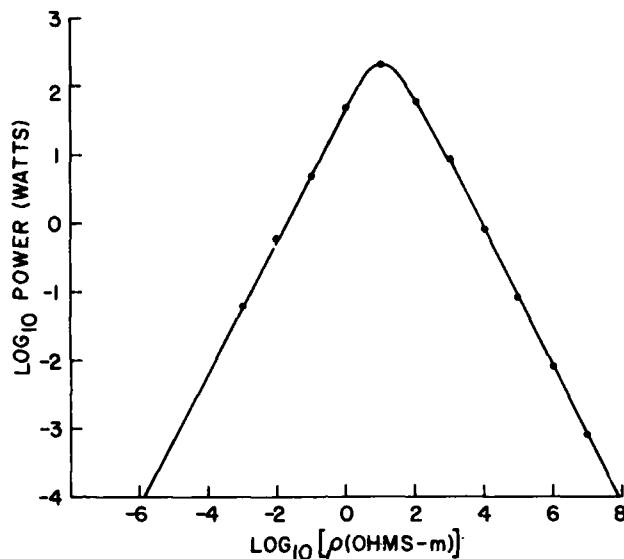


Figure 10. Ohmic Power Loss in Solar Power Satellite as a Function of Resistivity. The Solar Power Satellite is at $X_0 = 150$ km; plasma conditions are for Day 289, 1969

the earth's shadow, for the 21 ATS-5 plasma conditions and for $X_m = -150$. The points are contained by the lines $V_{\text{Drop}} = 0.06 V + 120$ and $V_{\text{Drop}} = 0.03 V$.

As V_{max} approaches zero, the electron current is dominated by the photoelectron current. Thus it appears that at $V_{\text{max}} = 0$ V there would be a minimum voltage drop dictated by the photoelectron current; that is, the differential photoelectron currents by themselves would drive ohmic currents which would determine the voltage drop. In practice, because V_{max} is zero, one end must have $V > 0$ and the photoelectron current becomes negligible. This explains the region of Figure 9 where the potential ~ 0 but the voltage drop is > 100 V. The last plot, Figure 10, is of the ohmic power dissipated through a structure as a function of the logarithm of resistivity. The value of resistivity for which the power is maximum has been empirically fit to a function of length and photoelectron current:

$$\rho_{\text{max}} = L^{-2} (J_p)^{-1/2} 10^{10.3}$$

where

$$L = \text{Length (km)}$$

J_p = photoelectron flux (A/m^2)

ρ = ohm-m

4. THEORETICAL FIT

Several of the preceding results can be theoretically explained as follows. Assume that a homogeneous plane structure of uniform thickness T and resistivity ρ is divided along a line of equal illumination into two sections (Figure 3b). The current through the interface is equal to the plasma current at equilibrium to either section

$$\int J_p(V, X) dA = \frac{dV}{dR} \quad (4)$$

Here, $J_p(V, X) dA$ is the differential current from the ambient environment to surface dA at potential V_x for $J_T(V_x) = 0 = J_p(V_x) + J_o(V_x)$; X is a coordinate system measured perpendicular to the interface and relative to the center of the structure, increasing in the direction of increasing illumination (Figure 3b); R is the resistance coordinate, increasing in the direction of increasing X (defined as $R = \int \rho/A dA$). Since

$$dA = L(X) dX \quad (5)$$

$$dR = \frac{\rho dX}{T L(X)} \quad (6)$$

where

$L(X)$ is the width of the structure at X ,

$$\int_{-S/2}^{X_1} J_T(V, X) L(X) dX = \frac{dV}{dX} \frac{T L(X)}{\rho} \quad (7)$$

S is the length of the structure parallel to the X axis; X_1 is the value of X at the interface.

Differentiating,

$$J_T(V, X) l(X) = \frac{d}{dX} \left(\frac{T L(X)}{\rho} \frac{dV}{dX} \right) \quad (8)$$

This may be rewritten as

$$\frac{\rho}{T} J_T(V, X) = D^2 V + g(X) D_X V \quad (9)$$

where

$$g(x) = \frac{dL(x)}{dx} \frac{1}{L(x)} \quad (10)$$

The left-hand side of Eq. (9) may be approximated by a Taylor's series:

$$J_T(V, X) \doteq J_T(V_1, X) + J_T'(V_1, X)(V - V_1) + J_T''(V_1, X) \frac{(V - V_1)^2}{2} \quad (11)$$

Because of the relative insignificance of the higher order derivatives of J_T (calculated numerically):

$$\frac{d}{dV} J_T(V, X) \doteq 10^{-10} \text{ A/Vm}^2$$

$$\frac{d^2}{dV^2} J_T(V, X) \doteq 10^{-14} \text{ A/V}^2 \text{m}^2$$

$$\frac{d^3}{dV^3} J_T(V, X) \doteq 10^{-18} \text{ A/V}^3 \text{m}^2$$

and so on,

all but the first two terms may be ignored for a result accurate to within first order for $|V - V_1| < 10^3 \text{ V}$

$$J_T(V, X) \doteq J_T(V_1, X) + \frac{d}{dV} J_T(V_1, X) (V - V_1) \quad (12)$$

Substituting in the value of V for which J_p is zero, namely V_z , we find:

$$J_T(V, X) \doteq \frac{d}{dV} J_T(V_z, X) (V - V_z) \quad (13)$$

Similarly, as V_z is a function of X and

$$\frac{d}{dX} V_z(X) \doteq 10^{-1} \text{ V/m}$$

$$\frac{d^2}{dX^2} V_z(X) \doteq 10^{-3} \text{ V/m}^2$$

and so on,

$$V_z(X) \doteq V_z(0) + \frac{d}{dX} V_z(0) X \quad (14)$$

Thus

$$J_T(V, X) = J'_T(V_z, X) (V - V_z(0) - V'_z(0) X) \quad (15)$$

Because $J''_T(V_z, X)$ is insignificant for the range considered,

$$J'_T(V_z, X) \doteq J'_T(V_z(0), 0) \quad (16)$$

$$J_T(V, X) = J_T(V_c, 0) (V - V_c - V'_z(0) X) \quad (17)$$

where

$$V_c = V_z(0) \quad , \quad \text{center of structure.} \quad (18)$$

Substituting Eq. (17) into Eq. (10),

$$\frac{\rho}{T} J'_T(V_c, 0) (V - V_c - V'_z(0) X) = D_x^2 V + (D_x V) g(x) \quad (19)$$

or, putting all references to V on the same side of the equation,

$$- \frac{\rho}{T} J'_T(V_c, 0) (V_c + V'_z(0) X) = (D_x^2 + g(x) D_x - \frac{\rho}{T} J'_T(V_c, 0)) V \quad (20)$$

we find that Eq. (20) can be solved using standard numerical techniques. However, if the width of the structure, $L(X)$, is a non-zero constant (SPS rectangular model), then $g(X)$ is zero, and Eq. (20) can be algebraically solved for V as a function of X :

$$V = \frac{c_1}{2} e^{(a_3 X)} + \frac{c_2}{2} e^{(-a_3 X)} + a_2 X + a_1 \quad (21)$$

where

$$\begin{aligned} a_1 &= V_c \\ a_2 &= V'_z(0) \\ a_3 &= (J'_t(V_c, 0) \rho / T)^{1/2} \end{aligned}$$

Assuming that $V(0) = V_c$,

$$V = c_1 \sinh(a_3 X) + a_2 X + a_1 \quad (22)$$

By Eq. (7) when $X = -s/2$, $dV/dX = 0$, and by Eq. (22),

$$\frac{dV}{dX} = c_1 a_3 \cosh(a_3 X) + a_2 = 0$$

so substituting $-s/2$ for X , we get a value of

$$c_1 = - \frac{a_2}{a_3 \cosh(-sa_3/2)} \quad (23)$$

Thus, the final equation for the SPS model is

$$V = a_4 \sinh(a_3 X) + a_2 X + a_1 \quad (24)$$

where

$$\begin{aligned} a_1 &= V_c \\ a_2 &= V'_z(0) \\ a_3 &= (J'_T(V_c, 0) \rho / T)^{1/2} \\ a_4 &= -a_2/a_3 \cosh(-sa_3/2) \end{aligned}$$

This equation fits the results of the numerical calculations, program SHADOW, to within approximately 10 percent. However, to achieve this accuracy,

it is necessary to have values of V_z' and J_T' for the plasma data used, and to stay within the ranges specified by the approximations used:

$$s < X_L$$

where X_L is the lowest value of X_M for any point on the structure, and

$$V_z(X) < 0 \text{ for all } X \text{ within the structure .}$$

The worst instances of charging were observed using data from Day 289, 1969, and from these data, values of 10^{-1} V/m and 10^{-10} A/Vm² for V_z' and J_T' were derived. These values may be taken to be a worst case.

5. CONCLUSION

The results of this study indicate that potential differences of 1,000 V across 10-km structures are possible under even the mild plasma conditions and with the relatively weak photoelectric current of the ATS-5 eclipses. Furthermore, engineers must be made aware of the effects of surface properties and resistivities of various spacecraft materials on spacecraft charging. One of these effects, previously unsuspected, is the existence of a resistivity for which the energy dissipation through a structure becomes a maximum and which is a function of length and photoelectron current density.

Four tools are provided the engineer for calculation of the voltages across a large space structure passing into eclipse: (1) the program SHADOW, which uses a detailed but efficient numerical algorithm; (2) differential Eq. (9) which may be solved using numerical methods; (3) Eq. (20), which can be solved with greater efficiency but with less accuracy; and (4) specifically for the SPS model, Eq. (24), which provides results with extreme efficiency and, so far as the limitation on shape takes it, the same accuracy as Eq. (20).

Because these methods ignore the effects of capacitance and inductance, they must be considered qualitative. However, knowledge of the potential and thus charge distribution can be used to estimate the former effects. Therefore, these techniques may prove an invaluable aid in predicting the charging effects on large space structures passing into eclipse.

References

1. DeForest, S.E. (1972) Spacecraft charging at synchronous orbit, J. Geophys. Res. 77(No. 4):651.
2. Garrett, H.B. (1977) Modeling of the Geosynchronous Plasma Environment, AFGL-TR-77-0288, AD A053 164.
3. Whipple, E.C. (1965) The Equilibrium Electric Potential of a Body in the Upper Atmosphere, NASA X-615-65-296.
4. Garrett, H.B., Pavel, A.L., and Hardy, D.A. (1977) Rapid Variations in Spacecraft Potential, AFGL-TR-77-0132, AD A046 350.
5. Rosen, A. (1975) Spacecraft Charging: Environment Induced Anomalies, Paper 75-91, AIAA 13th Aerospace Sciences Meeting.
6. Tsipouras, P., and Garrett, H.B. (1979) Spacecraft Charging Model - Two Maxwellian Approximation, AFGL-TR-79-0153, AD A077 907.
7. Rothwell, P.L., Rubin, A.G., and Yates, G.K. (1977) A simulation model of time-dependent spacecraft interactions, Proc. of the Spacecraft Charging Conference, AFGL-TR-77-0051/NASA TMX-73537.
8. Garrett, H.B., and Rubin, A.G. (1978) Spacecraft charging at geosynchronous orbit-generalized solution for eclipse passage, Geophys. Res. Lettrs. 5(No. 10):865.

Appendix A

Current Values as Functions of Voltage,
Number Density, and Temperature

CURRENT DENSITY EQUATIONS

For incident ambient electrons (or ions) the current density is the sum of the current densities of two populations where the current density for each population is:

$$J = J_0 \exp(-|qV|/kT) \text{ (for the repelled species)}$$

$$J = J_0 (1 + |qV|/kT) \text{ (for the attracted species)}$$

where J_0 is the population's current density at $V = 0$, q the charge of the particular species, and kT the Maxwellian temperature of a single population. The current densities of the secondary electron and backscatter electron fluxes, known collectively as the secondary current densities, are the sum of the secondary current densities caused by each of the primary populations; that is, the secondary electron current density is the sum of the secondary current densities caused by each of the two electron populations and the two ion populations, and the backscatter current density is the sum of the backscatter densities of the two ambient electron populations. On this population by population basis, the equations are relatively simple:

$$J_{sel} = J_{el} * a(V, T_{el})$$

$$J_{sil} = J_{il} * b(V, T_{il})$$

$$J_{bsl} = J_{el} * c(V, T_{el})$$

and so on,

where

$$\begin{aligned} a(V, T_e) &= 0 & V > 0 \\ &= 0.8431 + (-0.8424) \exp(-0.0286 * T_e) & V < 0, T_e < 200 \text{ eV} \\ a(V, T_e) &= 0.1431 + 0.665 \exp(-0.0003 * T_e) & V < 0, T_e > 200 \text{ eV} \\ c(V, T_e) &= 0.222 & V < 0 \\ &= (0.263 + (-0.0218) \exp(-0.00901 * V)) \\ &\quad + (0.11536 + (-0.00328) \cdot \exp(-0.15127 * V)) \\ &\quad \cdot \exp((-0.00081 + 0.00019 \exp(0.02217 * V)) * T_e) & V > 0 \end{aligned}$$

$$\begin{aligned} b(V, T_i) &= 0 & V > 0 \\ b(V, T_i) &= (4.78 - 0.6526 \exp(V * 0.9783 * 10^{-4})) \\ &\quad + (-0.5299 - 3.78 \exp(V * 0.1844 * 10^{-3})) \\ &\quad \cdot \exp(T_i * (-0.5715 * 10^{-4} - 0.1829 * 10^{-3} \\ &\quad \cdot \exp(0.1447 * 10^{-3} * V))) & V < 0 \end{aligned}$$

These values of a, b, and c have been calculated for aluminum. They have been multiplied by arbitrary coefficients to fit the ATS-5 observations (that is,

$$J_{se} = X \cdot J_e \cdot a, X = 1.3; J_{si} = Y \cdot J_i \cdot b, Y = 0.55; J_{bs} = Z \cdot J_e \cdot c, Z = 0.4).$$

The photoelectron current density is:

$$\begin{aligned} J_{pe} &= J_{peo} * F(X_m) & V < 0 \\ &= J_{peo} * F(X_m) * (1 + V/0.7)^{-2} & V > 0 \end{aligned}$$

when

J_{peo} is the saturation photoelectron current ($V = 0$, $X_m = 200$)

$F(X_m)$ is the fractional illumination of the spacecraft:

$$F(X_m) = 1 - \frac{\left(\frac{R_e}{R_s}\right)^2 (A - \sin A) + (B - \sin B)}{2\pi}$$

where

$$A = 2 \cos^{-1} \left(\frac{(X_m + R_E)^2 + R_E^2 - R_s^2}{2(X_m + R_E) R_E} \right)$$

$$B = 2 \cos^{-1} \left(\frac{(X_m + R_E)^2 + R_s^2 - R_E^2}{2(X_m + R_E) R_s} \right)$$

R_E = earth radius

R_s = apparent radius of sun at surface of the earth as seen by satellite.

As outlined in the Introduction, the different J's are computed for a given V. In the case of ohmic currents, J_{ohm} is given by:

$$J_{ohm}(X_i) = \frac{V(X_i) - V(X_{i-1})}{R} + \frac{V(X_i) - V(X_{i+1})}{R}$$

The potential V is then varied until either Eq. (3) or, for a single point, Eq. (2) is satisfied.

FORTRAN LISTINGS

Program Units

On the following pages are listed the iterative charging program SHADOW and its subprograms. SHADOW, itself, is only a blanket program directing the calls to data input and processing subroutines and performing data output directly. The first set of executable cards directs the input of plasma, structure, and other

parameters, with the option of calling either SBR or SPS for reading structure data. The next group is a DO loop which, for a series of structure positions, calculates voltages by calling CNVG and then prints the results.

Subroutine PLASMA reads the values of number density and temperature from which are calculated current density for both populations of each species, protons and electrons, and reads the photoelectron current density.

Subroutine MODEL determines the positions of the structure for which potentials are determined and stores values in common block ZERO.

Function CNORM determines current density from number density and temperature.

Subroutine SBR reads the dimensions, conductivity, and number of nodes of a circular structure and calculates the surface area of each node, the distance between nodes, and the conductance between nodes. Solar Power Satellite performs the equivalent operations for a square structure.

Function CURV determines the current to a structure as a function of potential and position on the first node, assuming current balance to all but the last node.

Function CURV is the net current to a node of potential VC and position X.

Subroutine CNVG finds the potential on each node. For low conductances, the method is to set each potential at the zero plasma value and then adjust potentials to counter current flow, eventually reaching equilibrium. For high conductances, the zero value of CURV is found, defining the values of array V.

Function ZERO finds the zero value of function FUNC.

Function DCDV finds the derivative of CURV with respect to V.

Function CT finds the total plasma current density to a node of potential V and position X.

Function CJPE is the photoelectron current density.

Function LNEX determines the value of $CHI(V)$.

Function BS determines the value of c.

Function SE determines the value of a.

Function SI determines the value of b.

Function FI is a service function for BS, SE, SI.

Function F determines the fraction of sunlight striking the spacecraft.

Subroutine AVG is a service function for function ZERO.

COMMON BLOCKS

For high efficiency, COMMON blocks are used for communication between subprograms. Thus, it is essential that their content be known to the programmer.

<u>Block</u>	<u>Variable</u>	<u>Purpose</u>
NP	NP	Number of nodes (points)
BOSTON	SEP	Separation between nodes (km)
	X	X_m for most illuminated node
	III	Service index variable for function CURV
	V(112)	Array of potentials (volts)
CON	CON (112)	Array of conductances between nodes (ohm^{-1})
ALL	CI	Ion population 1 current density (A/m^2)
	CE	Electron population 1 current density
	TI	Ion population 1 temperature (eV)
	TE	Electron population 1 temperature
	CP	Saturation photoelectron current density
TWOMAX	CI2	Ion population 2 current density (A/m^2)
	CE2	Electron population 2 current density
	TI2	Ion population 2 temperature
	TE2	Electron population 2 temperature
STRUCT	AREA (112)	Array of nodal surface areas (m^2)
GCON	GCON	Conductivity of structure ($\text{ohm}^{-1} \text{m}^{-1}$)
MATER	AA BB CC	Material-dependent secondary and backscatter emission coefficient
SHAPE	SHAPE	Value is 1 for spherical probe; 0 for plane surface
USE		

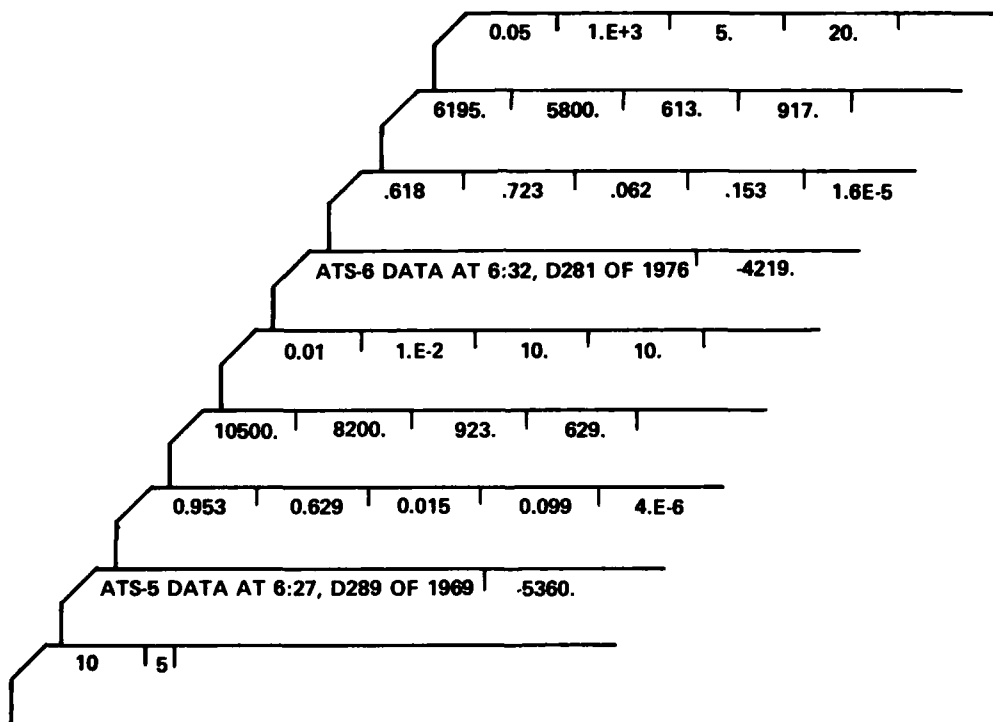
The first card of a data deck specifies the distance between spacecraft positions and the number of positions. The first value is in E 15.6 format and the next is in I4 format; the distance is in kilometers.

Next come the cards specific to each run: the cards specifying the plasma conditions and the structure parameters. The first card is a title card, with alphanumeric data in columns 1-57 and the spacecraft shadow potential in columns 58-80 in F22.10 format. In the listed version of SHADOW, the shadow potential is ignored.

The next card lists the plasma parameters: ion population 1 number density, electron population 1 number density, ion population 2 number density, electron population 2 number density, and photoelectron saturation current density; the number densities are in n/cm^3 , the current density is in A/m^2 . Next come the four population temperatures in eV: ion population 1 temperature, electron population 1 temperature, and so on. The values on the first card are listed in E15.5 format; on the second card, F15.5 format.

The last card for each run lists the thickness (m) and conductivity ($\text{ohms}^{-1} \text{m}^{-1}$) of the structure in E15.5 format, and the width or diameter (km) and number of nodes in F15.5 format.

Sample deck



```

PROGRAM SIADJN (INPUT, OUTPUT, TAPE9, TAPE5=INPUT, TAPE6=OUTPUT,
  DEBUG=OUTPUT)
EXTERNAL JT
DIMENSION XL(112), FFL(112), VSP(112), VR(112), /VSP(112),
1 VVGEN(112)
COMMON /NP/NP /BOSTON/SEP, X, III, V(112) 000790
1 /CONV/CON(112) /ALL/31, CE, F1, F2, CP
2 /ZERO/ACCUI, ACCU2/VC/VC(112) 000810
3 /TWOHXX/SI2, SE2, F12, F22 000815
4 /STRUCT/ AREA(112)/S2ON/ SCON
5 /MATER/ AA, BB, CC /SHAPE/ SHAPE
DIMENSION CUR (112), CNT (112), TIT.E(8) 000820
DATA SPERE, PLATE / 1., 0. /
AA = 1.3
BB = 0.4
CC = 0.55
3 READ MODEL DATA
CALL MODEL (DELTA, N)
2 CONTINUE
READ (5, 40) (TITLE(I), I=1,6), VAC
40 FORMAT (5A10, A7, F22.10)
IF (EOF(5) .NE. 0.) STOP 000920
WRITE (6, 41) (TITLE(I), I=1, 6), VAC
41 FORMAT (141, 5A10, A7, F10.2)
CALL PLATTA
SHAPE = P_PLANE
COLLECT DATA TO CALCULATE VOLTAGES ON A SQUARE STRUCTURE
CALL SPS
COMMENT IN ORDER TO CALCULATE THE VOLTAGES ON A ROUND STRUCTURE, USE STATEMENT
CALL SBR
V0 = ZERO (01, -299.)
WRITE (6, 70)
70 FORMAT (1H0, 15X, 5HCENTER, 5X, 5HLOCAL / 11X, 15(1H-), 24X,
1 65(1H-) / 3X, 24V0, 8X, 2H(4, 5X, 5HF(X4), 3X, 6HENERGY, 2X,
2 8HNET CJR., 6X, 24X4, 5X, 5HF(X4), 7X, 14V, 5X, 64V/V0, 6X,
1 3H44Z, 4X, 54441/4, 5X, 6HENERGY, 2X, 8HNET CJR., 2X, 9H04M. CUR.
* /)
II = 113 - NP
DO 1 I = 1, N 001040
X = -135.2 + FLOAT(I-1)*DELTA - 0.5*SEP
CALL CONV
XX = X - SEP*FLOAT(NP-1)/2.
9 FF = F(XX)
ENERGY = J.
OUT = J.
DO 11 J = 1, NP
III = J
XL(J) = X - FLOAT(J-1)*SEP
CJT = CJT + JT(VIJ), (L1J)*APEA(J)
CJ2(J) = CJR. (VIJ), (- FLOAT(J-1)*SEP)
FFL(J) = F(XL(J))
V2(J) = V(J)/V0
VSP(J) = V(1) - V(J)
IF (V(1).NE.V(NP)) VVSP(J) = VSP(J) / (V(1)-V(NP))
IF (J.EQ.NP) GO TO 10
CNT(J) = (V(J) - V(J+.)) * CON(J)
IF (CON(J) .EQ. 0.) J3 TO 10

```

THIS PAGE IS BEST QUALITY PRACTICABLE
FROM COPY FURNISHED TO DDC


```

ENERGY = ENERGY + ONT(J)**2/GON(J)
VVEN(J) = CNT(J)**2/GON(J)
10  CONTINUE
VCENSP = ENERGY
WRITE (6, 100) V0, XN, F, VVENSP, OUT, (X(-1*J+113),
* FFL(-1*J+113), V(-1*J+113), VR(-1*J+113), VS(-1*J+113),
* VVSP(-1*J+113), VVEN(-1*J+113), OUR(-1*J+113), ONT(-1*J+113),
* J = IT, 112)
100 FORMAT (1X, F7.1, F0.2, 1X, E10.3, F0.1, 1X, E10.3,
1 F5.2, 1X, E10.3, F0.1, F9.5, F3.1, 2E10.3, 2(1X, E10.3) /
2 1X, F0.2, 1X, E10.3, F0.1, F9.5, F0.1, 2E10.3, 2(1X, E10.3) )
IF (V(NP) .GT. 0.) GO TO 6
1  CONTINUE
6  CONTINUE
GO TO 2
GO TO 2
END

```

001220

001300

```

SUBROUTINE S33
COMMON /NP/NP /BOSTON/SEP
1 /GON/GON(11) /STRJST/AREA(112)
2 /GCON/GCON
READ (5, 100) THK, GCON, S, P
100 FORMAT (F15.5, 2E15.5, F12.5)
NP = P
WRITE (5, 101) THK, GCON, S, NP
101 FORMAT (110, 19HTHICKNESS (METERS) = , E12.3, 110)
1 26MCONDUCTIVITY (MHOS/METER) = , E12.3 /
1 14MWIDTH (CM) = ,
2 10.2, 13X, 27NUMBER OF POINTS IN MODEL = , I5 /)
SEP = S**3
CON(1) = GCON*THK/S / SEP
S = S*10.0
AREA(1) = S**2/P
ON 1 I=1, 112
CON(I) = CON(1)
1 AREA(I) = AREA(1)
RETURN
END

```

THIS PAGE IS BEST QUALITY PRACTICABLE
FROM COPY FURNISHED TO DDC

```

SUBROUTINE PLASMA
COMMON /STRUCT/ARFA(112)
1  /ALL/ OI, OE, TI, TE, 3P
2  /TWO MAX/ OI2, OE2, TI2, TE2
REAL KI, KE
DATA KI, KE / 1.24 F +5, 5.31 E + 6/
READ (5, 70) OI, OI2, OE, OE2, OI2, OI2, TI, TI2, TE, TE2
70 FORMAT (5 E 15.5 / 4 F 15.5)
OI = CNORM (OI, TI, KI)
OI2 = CNORM (OI2, TI2, KI)
OE = CNORM (OE, TE, KE)
OE2 = CNORM (OE2, TE2, KE)
OP = 1.E-5
WRITE (6, 72) OI, OE, OI2, OE2, TI, TE, TI2, TE2, OI, OE, OI2, OE2
1, OP
72 FORMAT (30HION NUMBER DENSITY (POP. 1) =, E12.4, 5X, 35HELECTRON N
1 NUMBER DENSITY (POP. 1) =, E12.4, 5X, 19H(NU1, 1043) /
2 30HION NUMBER DENSITY (POP. 2) =, E12.4, 5X,
3 35HELECTRON NUMBER DENSITY (POP. 2) =, E12.4 /
4 27HION TEMPERATURE (POP. 1) =, F12.4, 5X,
5 31HELECTRON TEMPERATURE (POP. 1) =, F12.4, 5X, 4H(NU1) /
6 27HION TEMPERATURE (POP. 2) =, F12.4, 5X,
7 31HELECTRON TEMPERATURE (POP. 2) =, F12.4 /
8 31HION CURRENT DENSITY (POP. 1) =, E12.4, 5X,
9 35HELECTRON CURRENT DENSITY (POP. 1) =, E12.4, 9H(AMPS/CM2) /
A 31HION CURRENT DENSITY (POP. 2) =, E12.4, 5X,
B 35HELECTRON CURRENT DENSITY (POP. 2) =, E12.4 /
C 32HOPHOTON ELECTRON CURRENT DENSITY =, E12.4 )
RETURN
END

```

```

SUBROUTINE MODEL (DELTA, N)
COMMON /ZERO/ ACCU1, ACCU2
READ (5, 50) DELTA, N
50 FORMAT (E 15.6, I4)
ACCU1 = 0.01
ACCU2 = 0.01
WRITE (5, 51) ACCU1, ACCU2, DELTA, N
51 FORMAT (1H1, 5HACCU1=, E13.6, 7H ACCU2=, E13.6, 7H DELTA=,
1 E13.6, 7H N=, I4 //)
RETURN
END

```

THIS PAGE IS BEST QUALITY PRACTICABLE
FROM COPY FURNISHED TO DDC

```

FUNCTION GNORM (S, T, K)
REAL K
GNORM = 1.
IF (T .LT. 5.) RETURN
GNORM = 5*SQRT(T)*K*5.0E-15*2.
RETURN
END

```

```

FUNCTION F(X)
DATA RE,PS/6378.,185.2/
F = 0.
IF (X .LE. (1.E-5)-RS) RETURN
F = 1.
IF (X .GE. RS-(1.E-6)) RETURN
A = 2.*4335*((X+RE)**2 + RE**2 - RS**2) / (2.*(X+RE)*RE)
B = 2.*4335*((X+RE)**2 + RS**2 - RE**2) / (2.*(X+RE)*RS)
F = 1. - (((RS**2)*(A-SIN(A)) + (B-SIN(B)))) / (3.1415926*2.)
RETURN
END

```

```

FUNCTION FI (V, AR)
DIMENSION AR(3)
IF (AR(2)*V .LT. 730.) GO TO 2
FI = AR(3) + AR(1)*1.E+10
RETURN
2 IF (AR(2)*V .GT. -50.) GO TO 1
FI = AR(3)
RETURN
1 FI = AR(3) + AR(1)*EXP(AR(2)*V)
RETURN
END

```

THIS PAGE IS BEST QUALITY PRACTICABLE
FROM COPY FURNISHED TO DDC

```

FUNCTION SI (V,T)
COMMON /WATER/ AA, BB, CC
DIMENSION A(3), B(3), C(3), D(3)
DATA A(1), A(2), A(3) / -.3733473E+1, .1844088E-3, -.5299395 /,
1 B(1), B(2), B(3) / -.12918E-3, .1446787E-3, -.5715818E-4 /,
1 C(1), C(2), C(3) / -.6526019, .9738416E-4, .4775591E+1 /
IF (V .GT. 0.) GO TO 1
D(1) = FI(V,1)
D(2) = FI(V,2)
D(3) = FI(V,3)
SI = FI(T,D) * CC
RETURN
1 SI = 0.
RETURN
END

```

```

FUNCTION SE (V, T)
COMMON /WATER/ AA, BB, CC
DIMENSION A(3), B(3)
DATA A(1), A(2), A(3) / -.8424, -.0256, .9431 /,
1 B(1), B(2), B(3) / .665, -.0003, .1431 /
IF (V .GT. 0.) GO TO 2
IF (T .LE. 236.) GO TO 1
SE = FI(T,B) * AA
RETURN
1 SE = FI(T,A) * AA
RETURN
2 SE = 0.
RETURN
END

```

```

FUNCTION SS (V, T)
COMMON /WATER/ AA, BB, CC
DIMENSION A(3), B(3), C(3), D(3)
DATA A(1), A(2), A(3) / -.00321, -.15127, .11536 /
DATA B(1), B(2), B(3) / .00013, .02217, .00001 /
DATA C(1), C(2), C(3) / -.02013, -.00901, .263046 /
DS = 2.777777 * BB
IF (V .LE. 0.) RETURN
IF (V .GT. 23.) V = 20.
D(1) = FI(V,1)
D(2) = FI(V,2)
D(3) = FI(V,3)
SS = FI(T,D) * AA
IF (SS .GT. 1.) SS = 1.
IF (SS .LT. 0.) SS = 0.
RETURN
END

```

THIS PAGE IS BEST QUALITY PRACTICE
FROM COPY FURNISHED TO SDC

```

REAL FUNCTION LNEK (VT)
COMMON /SHAPE/ SHAPE
IF (VT .LT. 300.) GO TO 3
IF (VT .LT. 500.) GO TO 2
IF (VT .LT. 3.) GO TO 1
LNEK = 1. + /T*SHAPE
RETURN
1 LNEK = EXP(VT)
RETURN
2 LNEK = 0.
RETURN
3 LNEK = VT + 1.E+10
RETURN
END

```

```

FUNCTION SJOE (V,X)
COMMON /ALL/ CI, C2, TI, T2, CP /SHAPE/ SHAPE
DATA SPHERE /1./
C = 1.
IF (SHAPE .EQ. SPHERE) C = 3.5
IF (V .LT. 0.) GO TO 1
SJOE = 3*F(X)*C
RETURN
1 SJOE = 3*F(X)/(1.+V*(0.7)**2) * C
RETURN
END

```

```

SUBROUTINE AVS (V, A, Q)
S = V
V = (V+A)/2.
RETURN
END

```

THIS PAGE IS BEST QUALITY PRACTICABLE
FROM COPY FURNISHED TO DDC

```

FUNCTION CT (V, X)
REAL LNE
COMMON /ALL/ CI, C2, TI, T2, CP /WOMAX/ C12, C22, T12, T22
CT1(V) = CJE(V) - CJI(V) - CJBSE(V) - CJSI(V) - CJSE(V) - CJPE(V, X)
1)
CJSE(V) = C2*LNE(V/TE)*SE(V, TE) + C22*LNE(V/TE2)*SE(V, TE2)
CJSI(V) = C1*LNE(V/TE)*SI(V, TI) + C12*LNE(V/TE2)*SI(V, T12)
CJBSE(V) = C2*LNE(V/TE)*BS(V, TE) + C22*LNE(V/TE2)*BS(V, TE2)
CJI(V) = C1*LNE(V/TE) + C12*LNE(V/TE2)
CJE(V) = C2*LNE(V/TE) + C22*LNE(V/TE2)
1 IF (ABS(V-0.5) .GT. 0.5) GO TO 2
CT = (CT1(1.) - CT1(3.))*V + CT1(0.)
RETURN
2 CT = CT1(V)
RETURN
END

```

```

FUNCTION DDD (V, I)
COMMON /CON/ CON(10) /STRUCT/ AREA(10) /NP/ NP
IF (I .NE. 1) GO TO 1
C0 = CON(1)
GO TO 3
1 IF (I .NE. NP) GO TO 2
C0 = CON(NP-1)
GO TO 3
2 C0 = CON(I) + CON(I-1)
3 DDV = C0 + AREA(I)*(CT(V+0.01, 0.) - CT(V, 0.))*10.
RETURN
END

```

```

FUNCTION ZER (FJND, X)
COMMON /ZERO/ ACCU1, ACCJ2
V = 0.
V1 = 0.
V2 = -20950.
6 C = FUND (V, X)
IF ((ABS(V1-V2) .LE. ACCU1) .AND. (ABS(C) .LE. ACCU2)) GO TO 3
IF (C .EQ. 0.) GO TO 4
CALL AVS (V, V2, V1)
GO TO 6
4 CALL AVS (V, V1, V2)
GO TO 6
3 ZERO = V
RETURN
END

```

```

SUBROUTINE G4V6
EXTERNAL CT, CJRL, CURV
COMMON /NP/NP, /BOBTON/SEP, X, II, V(1)
1 /ZERO/ACC1, ACC2/VS/VC(10)
2 /CON/ CON
* /STRUCT/ AREA(10) /CON/ CON(10)
* /TWO/OK/ OI2, OE2, FI2, FE2
IF (CON(1) .EQ. 0.) GO TO 12
I = 1
P = 1./CON(1)
DO 11 I = 3, NP
IF (CON(I-1) .EQ. 0.) GO TO 12
R = R + 1./CON(I-1)
11 CONTINUE
V(1) = ZERO(CT,X)
IF (CT/(1+.01,0.)-CT(V(1),0.))*AREA(1)*100.*R .LT. 5.0) GO TO
* 10
12 VS1 = 1.E+10
DO 1 I = 1, NP
1 V(I) = ZERO (CT, X-FLOAT(I-1)*SEP)
2 CONTINUE
NN = NP
DO 3 I = 1, NP
VC(I) = V(I)
II = I
V(II) = V(II) - CURL(V(II), X-FLOAT(II-1)*SEP)/DCDV(V(II), II)
* 0.5
II = NP+1-I
VC(II) = V(II)
V(II) = V(II) - CURL(V(II), X-FLOAT(II-1)*SEP)/DCDV(V(II), II)
* 0.5
3 CONTINUE
VS = 0.
DO 4 I=1, NP
4 VS = VS + (V(II) - VC(II))**2
IF (VS .LT. ACC2**2) GO TO 5
IF (VS .GT. V31-ACC2) GO TO 3
DO 6 I= 1, NP
6 V(II) = VC(II)
VS1=VS
GO TO 2
5 DO 5 I = 1, NP
5 V(II) = (V(II) + VC(II))/2.
VS1=VS
GO TO 2
6 CONTINUE
RETURN
10 CONTINUE
V(1) = ZERO(CURV, X)
RETURN
END

```

THIS PAGE IS BEST QUALITY PRACTICABLE
 FROM COPY FURNISHED TO DDC

```

FUNCTION CURL (V, X)
COMMON /NP/NP /CON/CON(10)
1 /BOSTON/SEP, XX, I, V(10)
2 /STRUCT/ AREA(112)
IF (I.NE. 1) GO TO 1
CURL = CT(V,1)*AREA(1) + (V-VC(2))*CON(1)
RETURN
1 IF (I.NE. NP) GO TO 2
CURL = CT(V,1)*AREA(NP) + (V-VC(I-1))*CON(NP-1)
RETURN
2 CURL = (V-VC(I-1))*CON(I-1) + (V-VC(I+1))*CON(I) + CT(V, X)*AREA(I)
1)
RETURN
END

```

```

FUNCTION CURV (V, X)
COMMON /CON/CON(1) /BOSTON/SEP, XX, I, V(1)
1 /NP/NP /STRUCT/ AREA(112)
V(1) = VC
V(2) = V(1) + CT(V, X)*AREA(1)/CON(1)
IF (NP.LT. 3) GO TO 2
DO 1 I = 3, NP
V(I) = (V(I-1)-V(I-2))*CON(I-2)/CON(I-1) + V(I-1) + CT(V(I-1),
1 *FLOAT(I-2)*SEP)*CON(I-1)*AREA(I-1)
1 CONTINUE
2 CURV = 0.
DO 3 I = 1, NP
3 CURV = CURV + CT(V(I), X*FLOAT(I-1)*SEP)*AREA(I)
RETURN
END

```

```

SUBROUTINE S33
COMMON /NP/ NP /BOSTON/ SEP
1 /CON/ CON(1) /STRUCT/ AREA(112)
2 /CON/ GCON
AINTG(X) = (SQRT(R*R-X*X) + R**2*ASIN(X/R))
DINTG(X, I) = AINTG(Y) - AINTG(X)
READ (5, 100) T4, GCON, R, P
100 FORMAT (2 E 15.5, 2 F 15.5)
NP = P
WRITE (5, 101) T4, GCON, R, NP
101 FORMAT (1H0, 19H THICKNESS (METER) = , E 12.3, 1)
1 26H CONDUCTIVITY (MHOS/METER) = , E 12.3 /
1 17H DIAMETER (CM) = ,
2 10.2, 10X, 27H NUMBER OF POINTS IN MODEL = , I5 /)
R = R*50.
SEP = 2.*R/P
DO 1 I=2, NP
X = -R + FLOAT(I-2)*SEP
AREA(I-1) = DINTG(X, X*SEP)
AREA IN 1*2
1 CON(I-1) = GCON*THICK*SQRT(R**2-(X*SEP)**2)*2./SEP
AREA(NP) = AREA(1)
SEP = SEP*100.
RETURN
END

```

THIS PAGE IS UNCLASSIFIED
 DATE 01/11/2001 BY 60320